

Pulse Width Evolution of Late Time X-rays Flares in GRBs

Daniel Kocevski ¹, Nathaniel Butler ^{1,2}, Joshua S. Bloom ^{1,3}

kocevski@berkeley.edu, nat@astro.berkeley.edu, j bloom@astro.berkeley.edu

ABSTRACT

We study the duration and variability of late time X-ray flares following gamma-ray bursts (GRBs) observed by the narrow field X-ray telescope (XRT) aboard the *Swift* spacecraft. These flares are thought to be indicative of late time activity by the central engine that powers the GRB and produced by means similar to those which produce the prompt emission. We use a non-parametric procedure to study the overall temporal properties of the flares and a structure function analysis to look for an evolution of the fundamental variability timescale between the prompt and late time emission. We find a strong correlation in 28 individual x-ray flares in 18 separate GRBs between the flare duration and their time of peak flux since the GRB trigger. We also find a qualitative trend of decreasing variability as a function of time since trigger, with a characteristic minimum variability timescale $\Delta t/t = 0.1$ for most flares. The correlation between pulse width and time is consistent with the effects of internal shocks at ever increasing collision radii but could also arise from delayed activity by the central source. Contemporaneous detections of high energy emission by GLAST could test between these two scenarios, as any late time X-ray emission would undergo inverse Compton scattering as it passes through the external shock. The profile of this high energy component should depend on the distance between the emitting region and the external shock.

Subject headings: gamma-rays bursts— X-rays: general — high energy:analysis

1. Introduction

One of the most unanticipated results to come from the *Swift* spacecraft (Gehrels et al. 2004) is the wide variety of X-ray behaviors observed in the early afterglows of gamma-ray

¹Astronomy Department, University of California, 601 Campbell Hall, Berkeley, CA 94720

²Space Sciences Laboratory, University of California, Berkeley, CA, 94720-7450, USA

³Sloan Research Fellow

bursts (GRBs). As of January of 2007, *Swift* had detected 206 GRBs and had observed a subset of $> 90\%$ of those events with the spacecraft’s narrow field X-ray telescope or XRT (Burrows et al. 2005). Of these events, $> 90\%$ show temporal properties that deviate from the simple post cooling break powerlaw decline that had been seen at late times ($\gtrsim 3 \times 10^4$ seconds) by previous spacecraft (e.g., Frontera et al. 2000; Gendre et al. 2006). Afterglows with simple powerlaw declines that extend from a few $\sim 10^2$ seconds to several days after a burst are seen, for example GRB 061007 (Mundell et al. 2006), but they constitute a far minority of the afterglows observed by the XRT. Instead, most afterglows show sharp drops in the observed flux immediately following the gamma-ray emission (Barthelmy et al. 2005a), lasting anywhere from $\sim 10^2$ to $\sim 10^3$ seconds post trigger. This is followed by a flattening of the light curve that can last hundreds of seconds (Granot, Knigl, & Piran 2006) before eventually transitioning to the late time powerlaw decay previous observed by other spacecraft. Most surprisingly, interspersed among these various components of the prompt afterglow emission have been the detections of major re-brightening episodes with emission flaring in some cases several hundred times above the declining afterglow emission (Burrows et al. 2005). In rare cases, these flares have actually surpassed the luminosity of the original GRB (Burrows et al. 2007).

Numerous papers have been published discussing a variety of mechanisms that could produce the late time flaring (Zhang et al. 2006; Liang et al. 2006; Falcone et al. 2006; Mundell et al. 2006; Perna et al. 2006; Proga & Zhang 2006; Lazzati & Perna 2007; Lee et al. 2007; Lyutikov 2006; Fan & Wei 2005). Most of these mechanisms place tight constraints on the timescales on which the their emission can be produced (Ioka, Kobayashi & Zhang 2005). The simplest explanation would be that the forward shock powering the afterglow runs into ambient density fluctuations as it moves into the surrounding medium (Wang & Loeb 2000). This external shock interpretation has difficulties explaining the degree of variability that is clearly seen in many of these flares (e.g., Burrows et al. 2005, and below). Simple kinematic arguments show that fluctuations due to turbulence of the interstellar medium or variable winds from the progenitor are expected to produce broad and smooth rise and decay profiles, with $\Delta t/t \sim 1$ (Ioka, Kobayashi & Zhang 2005). Here t is the time since the gamma-ray trigger and Δt is the variability timescale. Shocks internal to the relativistic outflow (Rees & Meszaros 1994; Narayan & Paczyński 1992), similar to the shocks believed to produced the prompt gamma-ray emission, do not suffer from these same constraints and could in theory produce variability on much shorter timescales. In the internal shock scenario the rise time of an individual pulse is governed by the time it takes for the reverse shock to propagate back through the shell. The decay time is largely set by the relativistic kinematics, or curvature effects, in which the arrival of off axis emission from a relativistically expanding shell is delayed and affected by a varying Doppler boost.

Another clue that the flares are produced in a region distinct from the external shock is that the temporal decay of the afterglow emission appears largely unaffected by the presence of flaring. The temporal index of the afterglow after the flaring activity is typically consistent with the pre-flare decay index. Although most bright flaring occurs within one hour of the GRB, flares have been observed during of each of the light curve phases described above. If, for example, the flare represented the onset of forward or reverse shock emission of a slow shell catching up and colliding with the external shock, then these flares would be expected to occur only before the flat energy injection phase. Furthermore, (Burrows et al. 2007) points out flaring in one example of a possible “naked burst“ (Kumar & Panaitescu 2000), an event which decays rapidly in time and therefore exhibits no evidence of external shock emission. This supports the argument that whatever is powering the afterglow is most likely not creating the X-ray flares, leaving internal shocks or direct central engine activity as likely methods for their production.

Further evidence that late time X-ray flares might be associated with internal shocks comes from their spectral characteristics. First, most of the flares are much harder than the underlying afterglow emission and, as reported by Burrows et al. (2007), the spectral characteristics of the afterglow emission appears unaffected by the flaring activity, possibly indicating two distinct emitting regions. Second, spectral fitting by Butler & Kocevski (2007) has shown that many flares can be well fit by the Band model (Band et al. 1993) that so effectively describes the prompt emission which is largely believed to be the result of internal shock collision. Furthermore, detailed time resolved spectral fitting of bright flares by Butler & Kocevski (2007) has shown that the spectral break energy E_{pk} of the Band model, which represents the energy at which most of the photons are emitted, evolves to lower energy during the flare in a way that is very similar to what is seen in the prompt emission (Norris et al. 1986). The evolution also follows the hardness-intensity correlation (Golenetski et al. 1983), a well known relationship observed in the prompt emission that can be attributed to the relativistic effects that produce the decay profile of individual pulses (Kocevski, Ryde & Liang 2003).

If the energy released by this activity is converted to radiation through late time internal shocks, then the question remains as to the characteristic radius that these internal shocks are occurring as well as the delay in their ejection. Either the central engine is still functioning and emitting shells at very late times, or the final few shells of the original outflow, which were emitted along with the shells that created the prompt emission, catch up with each other only after a long delay due to a small relative difference in their bulk Lorentz factor Γ . The first scenario could essentially produce shell collisions at any radius, as the delayed arrival of the flares would, in this case, primarily reflect the time that the engine was dormant (Kobayashi, Piran, & Sari 1997). The second scenario, predicts that the late time flares

should occur at a radius that is significantly larger than the radius at which the prompt emission was created, with their delayed arrival being a result of the shells’ time of flight before colliding. This second scenario leads to a very specific and testable prediction, namely that the width of individual pulses of emission should become broader and less variable when originating from shells of increasing collision radii R_c . Ramirez-Ruiz & Fenimore (2000) tested for this pulse width evolution in the light curve profiles of BATSE events and found no evidence for any such effect. They concluded that the prompt emission observed by BATSE must have been produced over a small range of R_c from the central engine and that no significant deceleration of Γ could have occurred over the duration of the observed activity.

The goal of this paper is to extend the gamma-ray pulse width analysis to the late time flaring X-ray emission following GRBs. The public catalog of *Swift* XRT flares (see also Chincarini et al. 2007) represents the first dataset to test the internal vs. external shock scenario for this flaring activity. Whereas previous studies were limited to prompt emission occurring less than 100 seconds after trigger, the late time X-ray flares give us the opportunity to test for pulse width and variability evolution out to, in some case, 1000 seconds after the trigger of the GRB where this effect may be more pronounced. We provide a simple derivation of the expected pulse width evolution in both small $\Delta\Gamma$ and delayed engine activity scenarios in §2, followed by a discussion of our data reduction techniques in §3 and results in §4. We find evidence for pulse width evolution in 28 flares as well as a qualitative trend of decreasing variability as a function of the flare’s time of peak flux. We discuss the implications of our observations in §5. This work expands upon and formalizes our previous reports (Kocevski, Butler & Bloom 2006; Butler 2007) of the discovery of pulse width evolution.

2. Pulse Width Evolution

The standard fireball model postulates the release of a large amount of energy by a central engine into a concentrated volume (Cavallo & Rees 1978), which causes the resulting outflow to expand and quickly become relativistic (Paczýnski 1986). In the internal shock scenario (Rees & Meszaros 1994), this outflow is assumed to be variable, consisting of multiple shells of differing bulk Lorentz factors Γ . These shells propagate and expand adiabatically until a faster shell collides with a slower one, causing the shells to coalesce and convert a significant fraction of their kinetic energy into radiation, most probably through optically thin synchrotron radiation. The resulting pulse profile that is observed is a convolution of two distinct timescales. The rise time of the pulse is largely due to the time it

takes for the reverse shock that is induced by the collision to cross the width of the faster shell. The decay time, on the other hand, is governed mainly by angular and kinematic effects where off axis emission is delayed and effected by a varying Doppler boost due to the curvature of the relativistic shell (see Figure 1 in Kocevski, Ryde & Liang (2003)). As a result, the decay time can be, and in most cases is, much longer than the rise time, leading to an asymmetric pulse profile. The combination of these two timescales (the shell crossing time and the angular time) naturally explains the so called “fast rise exponential decay” or FRED pulses that are so ubiquitous in prompt GRB emission.¹

If we examine these two timescales in more detail, we can see that the rise time is primarily a thickness effect and can be expressed as $\Delta t_{rise} = \delta R/c(\beta_2 - \beta_{rs})$, where δR and β_2 are the thickness and velocity of the second shell that is catching up to the first and β_{rs} is the velocity of the reverse shock. If both the slow and fast shells have Lorentz factors of roughly the same order $\sim \Gamma$, then the resulting rise time is of order $\sim \delta R/c$. Because the merging shells are traveling forward at a velocity very close to the speed of light ($\Gamma \gg 1$), the resulting coalesced shell keeps up with the photons that it emits. Therefore, any emission activity over a fixed duration will appear to an outside observer to be compressed in time by a factor of $1/2\Gamma_m^2$, where Γ_m is the resulting Lorentz factor of the merged shell. The observed rise time can therefore be written as

$$\Delta t_r \approx \frac{\delta R}{2c\Gamma_m^2} \quad (1)$$

So given a sufficiently large Γ_m , internal shocks can essentially produce variability along the line of sight on arbitrarily short timescales.

Angular (or curvature) effects have the opposite effect, causing a broadening of the overall emission profile that can quickly come to dominate the observed pulse shape. The decay timescale is essentially the difference in light-travel time between photons emitted along the line of sight and photons emitted at an angle θ along a shell of radius R . This can be stated as

$$\Delta t_d = \frac{R(1 - \cos \Delta\theta)}{c} \approx \frac{R(\Delta\theta)^2}{2c} \approx \frac{R}{2c\Gamma^2} \quad (2)$$

Where the last step assumes that the shell is moving with sufficient velocity such that the solid angle accessible to the observer is limited by relativistic beaming and thus given by $\Delta\theta \sim 1/\Gamma^2$. Therefore comparing Equation 1 and Equation 2, we can see that curvature

¹Here we assume that the intrinsic cooling time Δt_c of the shell is insignificant compared to the duration of the shell crossing Δt_r and angular Δt_d timescales because of the magnetic field strength required to produce the gamma-ray emission

effects become important whenever the radius of the shell exceeds the shell thickness, which is true for all but the earliest moments of the shell’s expansion.

The significance of Equation 2 is that angular effects should scale linearly with the radius of the emitting shell and therefore pulse durations should become broader as shell collisions occur further from the central engine. If the flares are the result of multiple shells that have been ejected almost instantaneously (or at least within a timescale that is small compared to the overall GRB duration) but collide at very late times due to a small dispersion in Lorentz factors, then one would expect that these late collisions would occur at greater radii. In this scenario, we can replace the radius of the shell in Equation 2 with the time t since the ejection of the first shell by noting that the observed radius of a spherical shell expanding with $v \sim c$ can be approximated as $R \approx ct\Gamma^2$, where the extra factor of Γ^2 is due to relativistic corrections, leading to

$$\Delta t_d \approx \frac{t}{2} \quad (3)$$

Therefore, the late shock scenario would predict a linear correlation between a shell’s time of flight and the resulting pulse duration, independent of the Lorentz factor of the shell. This relationship between the pulse duration the time since the ejection of the internal shocks has been noted before. Fenimore, Madras, Nayakshin (1996) found, through a much more detailed derivation, that a pulse’s *FWHM* should scale roughly as $0.26T_0$ to $0.19T_0$ as the low energy powerlaw index α varies from 1 to 2. Similarly, Ioka, Kobayashi & Zhang (2005) derive that the variability of flares that result from refreshed shocks should be limited by $\Delta t \geq t_p/4$. In each case, flares occurring at larger radii are expected to produce broader pulse durations.

This relationship between Δt_d and t is modified if there is an intrinsic delay Δt_{engine} in the ejection of the subsequent shells by the central engine. If we imagine two shells emitting at time zero and time Δt_{engine} , provided the Lorentz factor of the second shell $\Gamma_2 > \Gamma_1$, the Lorentz factor of the first shell, the shells will collide at time

$$t_c = \frac{\Gamma_1^2 \Delta t_{engine}}{\Gamma_2^2 - \Gamma_1^2} \quad (4)$$

If the the shells have equal mass, which corresponds to the maximal efficiency for conversion of kinetic energy into radiation, energy and momentum conservation lead to a merged shell with Lorentz factor $\Gamma_m = \sqrt{\Gamma_1 \Gamma_2}$. The timescale over which the shell emits will be governed by the longest timescale of Δt_a , Δt_r , or Δt_c , the angular, the radial, or the cooling timescale, respectively. The angular and radial timescales can both be given as:

$$\Delta t_a \approx \Delta t_r \approx \frac{R}{2c\Gamma_m^2} = \frac{R}{2c\Gamma_1\Gamma_2}. \quad (5)$$

The time at which a flare is observed will be t_c , and the observed duration will be $\Delta t = t_c\Gamma_1/\Gamma_2 \approx t_c/2$ for an efficient collision with $\Gamma_2 = 2\Gamma_1$. For this Γ_2/Γ_1 ratio, the flare duration Δt is related to the duration at the central engine by $\Delta t = \Delta t_{\text{engine}}/6 \sim \Delta t_{\text{engine}}$. Therefore, if there is any appreciable delay in the ejection of relativistic material from the central engine, the resulting pulse shape will not necessarily reflect the shell radius, but rather the intrinsic delay between the ejection of the two shells. Any correlation between pulse shape and time of peak flux must then be attributed to the activity of the central engine.

3. Data & Analysis

We select a subsample of 28 bright ($\gtrsim 10$ cts/s) flares that are fully time-sampled (i.e., no gaps in their light curves) in 18 separate GRB afterglows observed by XRT. The Burst Alert Telescope (BAT) and XRT data were downloaded from the *Swift* Archive² and processed with version 0.10.3 of the `xrtpipeline` reduction script and other tools from the HEASoft 6.0.6³ software release. We employ the latest (2006-12-19) calibration files available to us at the time of writing.

The reduction from cleaned event lists output by the `xrtpipeline` code and from the HEASoft BAT software to science ready light curves and spectra is described in detail in Butler & Kocevski (2007). The bright XRT flare data are taken overwhelmingly in windowed-timing (WT) mode, which mandates special attention to bad detector columns. As the spacecraft moves, a significant and time varying fraction of the source flux can be lost if source counts fall on the bad columns. To account for this (see, Butler & Kocevski 2007), we calculate exposure maps for the WT mode on a frame-by-frame basis. We accumulate 0.3-10.0 keV counts in each light curve bin until a fixed signal-to-noise (S/N) of 3 is achieved. All of the resulting light curves to which we apply our analysis are publicly available⁴. A composite light curve plot showing all 18 GRBs in our data set is shown in Figure 1.

²<ftp://legacy.gsfc.nasa.gov/swift/data>

³<http://heasarc.gsfc.nasa.gov/docs/software/lheasoft/>

⁴<http://astro.berkeley.edu/~nat/swift>

3.1. Flare Duration Measures

The first step in our analysis consists of measuring the global flare duration timescales. Because we have found no one functional form (e.g., Gaussians) to adequately fit the X-ray flare time profiles (Figure 1), we employ non-parametric duration estimators. We consider the flare T_{90} duration as the time required to accumulate between 5% and 95% of the flare counts. We also define a rise time as the time between 5% accumulation and the time of count rate peak. Errors on these quantities are determined from the non-parametric bootstrap (i.e., by recalculating the quantities for data simulated using the measured data and errors).

A bias affecting these duration measures (and probably all durations measures) is the unknown background under the flares. As discussed above, studies have shown that a power-law decaying background likely does exist. However, it cannot cleanly be measured in many of our events and not at all for events which suffer from data gaps. In an effort to avoid such biases in our duration measurements, we have restricted our analysis to flares that are typically 2–3 orders of magnitude above background.

3.2. Flare Variability Measures

The flare duration and the component rise and decay times are gross measures of variability. In addition to this information, we attempt to measure the finer timescale fluctuations in the light curves which may prove important for inferring the size and nature of the flare’s emitting region. Several methods for measuring signal power versus time scale have been applied to astronomical inquires and in GRB research in particular. Several authors (e.g., Belli 1992; Giblin, Kouveliotou, & van Paradijs 1998; Beloborodov, Stern, & Svensson 2000) employ the Fourier power spectral density (PSD) to study time variations in GRB light curves. The autocorrelation function (ACF), which is simply the Fourier transform of this PSD, has been used to demonstrate a narrowing of GRB pulses with increasing energy band (e.g., Fenimore et al. 1995). Below, we utilize the *first order structure function*, which is directly proportional to the ACF and has a rich heritage in the study of quasar time histories (e. g., Simonetti, et al. 1985; Hughes, Aller, & Aller 1992).

Because the light curves of flaring sources are by definition non-stationary signals (i.e. signals whose frequency content changes with time) which exhibit sharp discontinuities, Fourier transforms do a particularly poor job of accurately measuring their power on both short and long timescales. Furthermore, they offer no ability to distinguish the temporal variations of specific spectral components (i.e. the time at which a characteristic frequency changes in a light curve) They are also somewhat more prone than *ACF* methods to aliasing

effects due to irregularly time-sampled data.

Instead of constructing a PSD using superpositions of sines and cosines, we can perform the equivalent analysis by constructing a scaleogram through the use of a discrete Haar wavelet transform. The Haar wavelet is the simplest possible wavelet, consisting of a step function, and has been previously exploited to “denoise” GRB light curves (e.g., Kolaczyk & Dixon 2000) and to infer milli-second variability during the first seconds of bright BATSE GRB (Walker, Schaefer & Fenimore 2000).

As described in more detail in the Appendix, we calculate the structure function from Haar wavelet coefficients as:

$$\sigma_{X,\Delta t}^2 = \Delta t/t \sum_{i=0}^{t/2\Delta t-1} (\bar{X}_{2i+1,\Delta t} - \bar{X}_{2i,\Delta t})^2. \quad (6)$$

where X_i is the natural logarithm of the observed XRT count rate in bin i at time t , and Δt is the timescale (or time “lag”) between successive bins. The bar over the X_i denotes an averaging with respect to shorter timescales, which is accomplished by the discrete wavelet transform (see, e.g., Press et al. 1992). If this averaging were not performed, $\sigma_{X,\Delta t}^2$ would be equal to the structure function $SF = \langle (X_{i+\Delta t} - X_i)^2 \rangle = 1 - ACF$. Instead, we have an estimator for SF , which ends up being far easier to interpret, as we discuss in the Appendix.

4. Results

4.1. Pulse Broadening in an Individual Event

A composite BAT and XRT light curve for GRB 060714 is shown in Figure 2. The red solid line represents a multiply-broken powerlaw fit to the light curve. The inflection points in the fit allow us to measure the boundaries and durations of the individual pulses within the signal. Each pulse is delineated by the short-dotted lines with the corresponding pulse duration labeled below the light curve. A general trend can be seen in which the pulse durations become broader as the burst progresses, with the shortest activity occurring early in the event.

The bottom panel plots the minimum timescale Δt for which $\sigma_{X,\Delta t}$ is at least 3σ above the floor expected from Poissonian fluctuations. Consistent with the trend seen in pulse duration, this minimum variability timescale, which is calculated without fitting the data, increases roughly as a powerlaw as the burst moves from early gamma-ray emission to late X-ray emission. To show that this increase in the variability timescale is not simply due to an increase in the data binning as the burst fades, we have plotted the time binning as a

short dotted line in the bottom panel. For most of the event ($t \lesssim 200$ seconds), the timescale below which little or no significant power exists is at least an order of magnitude higher than the resolution of the light curve allowed by the binning of the signal. Overall, the bottom panel shows that the very fast time variability associated with the prompt GRB emission dies out at late times.

Although the general broadening of the pulse durations seen in Figure 2 can be detected within the separate BAT and XRT light curves, the comparison of the pulse durations can only be qualitative when considering a light curve that spans both detectors. This is because GRBs are typically wider at lower energies (Fenimore, Madras, Nayakshin 1996), a direct result of the evolution of their spectral break energy E_{pk} to lower energies. We shown in Butler & Kocevski (2007) that the X-ray flares typically have E_{pk} in the X-ray band, while the earlier GRB emission has E_{pk} in the gamma-ray band. Therefore pulses are expected to be intrinsically broader in the 0.3–10.0 keV bandpass of the XRT than the higher 10–100 keV observed by BAT.

4.2. Pulse Broadening in the Sample Taken as a Whole

To eliminate the pulse broadening between separate energy bands, we limit our quantitative comparison of pulse durations (both within a single GRB and across our entire sample) to measurements made using only the XRT data on each event. This comparison is shown in Figure 3, where we plot pulse duration versus time of peak flux for our entire sample of XRT observed GRBs. The flares associated with each GRB are represented by the same color and symbol, with several GRBs exhibiting multiple flares throughout their early afterglow.

As a whole, the sample shows a clear correlation between the flare duration and the time of peak flux since the GRB trigger. The resulting correlation strength is Kendall’s $\tau_K = 0.7$, with a significance of 10^{-7} . The slope is consistent with linear, implying $\Delta t \propto t_p$, which cancels out the effects of cosmological redshift. We find no significant correlation between duration and redshift ($\tau_K = 0.2$, signif.= 0.2), further ruling out cosmological time dilation as the source of this correlation.

Roughly, half of the events with multiple flares (those plotted in color in Figure 3) show a trend toward increasing duration with observation time. The other half show an anticorrelation. The pulse durations, time of peak flux, and rise times for al the flares in our sample can be found in Table 1.

4.3. Haar Structure Function View

Figure 4 shows $\sigma_{X,\Delta t}$ versus Δt and $\sigma_{X,\Delta t}$ versus $\Delta t/t$ for the ensemble of flares under study⁵. In this scaleogram plot, we show only 3σ excesses over the power associated with Poisson fluctuations and report lower values as 3σ upper limits.

An X-ray flare is an emission episode uncorrelated in time to the afterglow flux prior to and after the flare. During the flare and on timescales short relative to the flare duration, the flux will be highly correlated in time and there will be a linear rise in $\sigma_{X,\Delta t}$. This can be observed to arbitrarily short timescale if the fading powerlaw tail of a flare is measured with very high S/N . On the other hand, as we describe in more detail in the appendix, correlated behavior in the light curve flattens the structure function, and this provides a direct measure of the flare timescales.

Consistent with the pulse duration correlation seen in Figure 3, the scaleogram plots show a range of important flaring timescale $dt = 30 - 300$ s, which becomes much tighter in units $dt/t = 0.1 - 0.5$. We observe a minimum characteristic timescale $dt/t = 0.1$.

The fractional flux variation levels at the minimum timescale are large ($\sigma_{X,\Delta t} \gtrsim 80\%$), suggesting that the variations correspond to gross features in the light curve. Consistent with this interpretation, we observe the flare rise times to have $\Delta t_{\text{rise}}/t = 0.1$ on average (Figure 8), and it is likely the sharp flare rises which produce the shortest timescales reflected in the structure function turnover. From the linear $\sigma_{X,\Delta t}$, we can rule out significant flickering on timescales shorter than $dt/t = 0.1$ (or $dt = 30$ s) at very small $\gtrsim 3\%$ fractional flux levels (Figure 3). We discuss the flare noise properties as a function of timescale in more detail in Butler, Kocevski & Bloom (2007).

For observation times in the 100 to 1000 second range, $dt/t = 0.1$ implies emission radii $R_c \approx 10^{15} \text{ cm} - 10^{16} \text{ cm}$, for a bulk Lorentz factor $\Gamma = 100$ (Equation 1). The observable emission is restricted to an angle $\approx 1/\Gamma$, implying an effective emitting region of size $\delta R \approx R_c/\Gamma \approx 10^{14} \text{ cm} - 10^{15} \text{ cm}$, compared to the typical external shock values of 10^{16} cm in the first hour or so (Piran 1999).

⁵We reserve a more detailed study of the Haar structure functions of individual flare events and *Swift* GRBs in a separate paper (Butler, Kocevski & Bloom 2007).

5. Discussion

The results from the temporal analysis outlined above provide substantial evidence that both the pulse duration and pulse variability of late time X-ray flares evolve with time. Both the pulse duration and variability timescales appear to have a narrow intrinsic range in $\Delta t/t = 0.3 \pm 0.2$, consistent with a narrow range found independently by Burrows et al. (2007) for Δt_{rise} and by Chincarini et al. (2007) for T_{90} . GRB 060714 provides the best example of this behavior in an individual event. Several other individual GRBs display a similar increasing pulse duration trend among their associated flares, although several bursts do not (e.g., GRB 060210). For the bursts with multiple flares, only half show increasing flare durations. Each burst event typically shows only 1, sometimes 2 (and 3 in one case) separate flares. These multiple flares within individual GRBs are only weakly separated in logarithmic time, and hence probe a small range of R_c or t_{engine} which may not allow for a clean measurement of time evolution in individual events.

The linear relationship between Δt and t_p is consistent with the pulse width evolution that is expected from the angular effects of late internal shocks at large radii as outlined in §2. Because we do not see a significant alteration of the afterglow light curve after the occurrence of an X-ray flare, the standard refreshed shock model, in which the trailing shells catch up to the leading shell only after the leading shell decelerates due to an external medium, is disfavored. Although such a scenario is expected to produce a correlation between the pulse width and time of peak flux on the order of $\Delta t \geq t_p/4$ (Ioka, Kobayashi & Zhang 2005), the trailing shells should have the effect of increasing the overall afterglow energy and thus have a discernible effect on the afterglow light curve, which is not seen. Therefore, the internal shocks producing the flares would have to be occurring behind the leading shock that has begun powering the afterglow, with their late occurrence, in this scenario, being due to a small relative Lorentz factor between the two inner shells.

The primary difficulty with this interpretation is the high flux ratio between the prompt and late emission, given the relatively small $\Delta\Gamma$ needed to explain the late collision time. As shown in detail by Krimm et al. (2007), the efficiency ϵ of an internal shock in converting a system’s kinetic energy into radiation scales roughly as $\epsilon \sim \Delta\Gamma^2$, so the observed flux drops quickly as the contrast between the Lorentz factor of the shocks decreases. This poses a problem for the flares observed by Swift, as many exhibit peak fluxes that are significant fractions of, and in some cases comparable to, their associated prompt emission. The small $\Delta\Gamma$ scenario would require an extremely large total amount of kinetic energy to remain in the system after the release of the prompt emission, given the low efficiency of the late collisions. These late and highly energetic shocks would, after producing the flaring activity, eventually collide with the external shocks and affect the observed afterglow light curve, something that

is not seen in all events with flares.

Alternatively, if the late nature of the X-ray flares is due to a significant delay in the ejection of late shells by the central engine, then the necessity of a small $\Delta\Gamma$ is eliminated, alleviating this efficiency constraint. As described in §2, the arrival time t_c and pulse width Δt would then directly reflect the activity of the central engine. Therefore, in this scenario, the correlation between t_c and Δt would require an explanation intrinsic to the powering and/or reactivation of the central engine at late times. Several authors have suggested mechanisms by which the central engine could be active at late times, most involving late-time fallback material or a long lived accretion disks around a central black hole. A model proposed by King et al. (2005) suggests that the late-time activity could be attributed to the fragmentation and accretion of a collapsed stellar core resulting in a sporadic release of energy rather than the classic view of a single cataclysmic event. Similarly, Perna et al. (2006) have proposed a viscous disk model in which the late-time activity is due to re-energization by material that falls in from a range of initial radii toward the accreting black hole. In this scenario, the correlation between t_c and Δt would be due to the range of radii from which the accreting material was falling. Material at large radii, if continuously distributed throughout its orbit, would take longer to fall back onto the central black hole and would do so over a longer duration, due to its larger orbital circumference.

These models are not without their own share of difficulties. The simple fragmentation models (King et al. 2005) are inconsistent with the implication of the spectral evolution seen in many flares (Krimm et al. 2007). Similarly, the viscous disk model requires a continuous distribution of material at discrete orbits to account for the episodic nature of the flares as well as an extremely long lived, and hence low viscosity, accretion disk to explain flares at 1000 seconds after the original collapse.

It cannot be completely ruled out that the observed time evolution is due to spectral evolution or the superposition of multiple flares. Consider 060124 (Butler & Kocevski 2007; Romano et al. 2006), in which the flares may in fact be the prompt emission, because the faint BAT trigger may be a pre-cursor. At high energies, the first XRT “flare” resolves into 2–3 shorter timescale BAT flares, which are blurred together in the XRT. We note that a shift of time origin for 060124 from $t \sim 0$ s to $t \sim 300$ s, corresponding to a shift in origin from the pre-cursor to the flare start, does not lead to a violation of the Δt and t_p correlation. Although, if we used the BAT flare durations, the correlation could be violated.

This indicates that spectral considerations are important, and that we are likely measuring in the XRT (in some cases) a pulse superposition. The duration which increases in time still appears to measure the duration of major emission activity, however, it is not clear that these are individual pulses. We know that spectra of late time flares are evolving strongly

(Butler & Kocevski 2007) during the flares. However, we observe only a weak correlation between peak time and hardness, indicating that there is a diversity of flare spectra at each epoch.

Another important concern involves the powerlaw background onto which most of these flares are superimposed. Although we have not attempted to subtract the background from the events in our sample (because the backgrounds are not well defined), this should not dominate the observed correlation. We have selected the brightest flares for analysis, which have peak fluxes orders of magnitude greater than the underlying background flux. The correlation is also strong for measures of duration like T_{50} or the Reichart et al. (2001) T_{45} , which are largely insensitive to pulse tails. Finally, we note that the flare rise time also strongly correlates with the peak time t_p as shown in Figure 5.

Barring any of these selection and/or analysis effects and assuming that the pulse width evolution is real, one possible test to distinguish between the late internal shocks with small contrasts $\Delta\Gamma$ and direct central engine activity may come from contemporaneous high energy emission during the X-ray flares. If the internal shocks creating the flares are occurring behind the external shock, then one would expect the X-ray photons to be boosted to higher energies by a factor of Γ_{FS}^2 through inverse Compton (IC) scattering as they pass through the external shock (Rybicki & Lightman 1979). The soft X-ray 10 KeV photons associated with the X-ray flares could easily be boosted into the 1–100 MeV range depending on the Lorentz factor of the external shock. The temporal profile of this high energy component should depend heavily on the distance behind the external shock at which this emission originated (Wang, Zhuo, & Mészáros 2000), as the duration of the IC component will reflect the geometry of the external shock, roughly $R/2\Gamma^2c$. The ratio between the flare duration and the IC component’s duration should approach 1:1 as the radius of the internal shock producing the flare approaches the external shock radius. Internal shocks that result from delayed central engine activity do not necessarily have to be at large radii to produce the longer observed durations. Therefore, larger IC component to flare duration ratios are expected for flares produced from small radii collisions. Even if these late-time collisions at small radii have intrinsically longer durations, as suggested by late central engine activity models, the additional light travel time from the origin of the late time flares to the external shock as it expands may make this change in duration ratios measurable. Such a test for contemporaneous high energy emission will be aptly suited for the upcoming GLAST mission which will be sensitive to photons up to > 300 GeV.

6. Acknowledgments

D.K. acknowledges financial supported through the NSF Astronomy & Astrophysics Postdoctoral Fellowships under award AST-0502502. N.B. gratefully acknowledges support from a Townes Fellowship at U. C. Berkeley Space Sciences Laboratory and partial support from J. Bloom and A. Filippenko. J. S. B. and his group are partially supported by a DOE SciDAC Program through the collaborative agreement DE-FC02-06ER41438. We also thank Phil Chang, Edison Liang, and Demos Kazanas for their thoughtful discussion.

7. Appendix

We describe here the mathematical representation of a Haar wavelet and its use in the construction of a scaleogram closely related the the *ACF* and first order structure function *SF*.

Given T successive data bins X_i , we define the Haar wavelet coefficients $h_{i,1}$ on scale $\Delta t = 1$ as

$$h_{i,1} = X_{2i+1} - X_{2i}, \quad i = 0, \dots, T/2 - 1. \quad (7)$$

At the same time, we can calculate the signal smoothed over a 2 bin scale $\Delta t = 2$:

$$\bar{X}_{i,2} = \frac{1}{2}(X_{2i+1} + X_{2i}), \quad i = 0, \dots, T/2 - 1. \quad (8)$$

By successively differencing and smoothing the signal on dyadic scales $\Delta t = 1, 2, 4$, etc., we build up the discrete Haar transform (see, also, Press et al. 1992):

$$h_{i,\Delta t} = \bar{X}_{2i+1,\Delta t} - \bar{X}_{2i,\Delta t}, \quad i = 0, \dots, T/2\Delta t - 1. \quad (9)$$

If the X_i are uncorrelated with equal variance, then the $h_{i,\Delta t}$ will be approximately linearly independent. We form a Haar scaleogram by averaging the $h_{i,\Delta t}$ at each scale Δt :

$$\sigma_{X,\Delta t}^2 = \Delta t/t \sum_{i=0}^{t/2\Delta t-1} h_{i,\Delta t}^2 = \Delta t/t \sum_{i=0}^{t/2\Delta t-1} (\bar{X}_{2i+1,\Delta t} - \bar{X}_{2i,\Delta t})^2. \quad (10)$$

In practice, we calculate this average as an average weighted by the data measurement uncertainties, $w_i = 1/\sigma_{D,i}^2$.

This quantity, also known as the Allan (1966) variance, is closely related to the structure function $SF = \langle (X_{i+\Delta t} - X_i)^2 \rangle$, where $\langle \dots \rangle$ denotes an average over the data. Unlike $\sigma_{X,\Delta t}^2$ the quantity SF is calculated without averaging the data on scale Δt before differencing

on that scale. This leads to a scaleogram with correlations (even for uncorrelated input data) between nearby data bins. The uncorrelated scaleogram $\sigma_{X,\Delta t}^2$ is therefore easier to fit and interpret, while both scaleograms have similar shapes for a wide variety of noise models.

7.1. Flare Ensemble Haar Structure Function

Because the Haar wavelets encode signal scale information as a function of time, it is possible to calculate $\sigma_{X,\Delta t}^2$ for arbitrary time sections of a light curve (e.g., Figure 2) or for the full light curve.

To make useful scaleogram plots for multiple GRB flares (e.g., Figures 4), we place the times series data end-to-end and perform the Haar transform as though the data were binned on an even time grid. Transform coefficients formed by differencing data from separate events are discarded. By saving the actual time since GRB trigger t and time bin width Δt for each wavelet coefficient, we can then rebin the coefficients in time on a dyadic grid starting with the minimum bin size. In this fashion, it is possible to plot statistically independent $\sigma_{X,\Delta t}$ points versus the physically meaningful Δt or $\Delta t/t$.

For X_i in Equations 7–9, we use the natural logarithm of the XRT count rate. Because the counts have been binned to a fixed S/N ratio, the error in X_i is approximately constant ($\sigma_D \approx 1/3$). The natural logarithm is also useful because powerlaw flux variations lead to a “zero-flaring” scaleogram with $\sigma_{X,\Delta t} \propto \Delta t$, as can be seen from a Taylor expansion of the flux in time. Also because we are working with the logarithm of the count rate, $\sigma_{X,\Delta t}$ can be interpreted as a root-mean-square (RMS) fractional variation in the flux F (i.e., $\delta X \approx \delta F/F$).

7.2. Structure Function Interpretation

Following the discussion in Hughes, Aller, & Aller (1992), on short timescales, the scaleogram $\sigma_{X,\Delta t}$ asymptotes to σ_D , where σ_D is the data measurement uncertainty. Because we know σ_D , we can subtract this flattening out. (This is typically not possible for SF due to the introduction of correlations in the data.) From the Cauchy-Schwarz inequality⁶, the scaleogram increases with increasing time lag. It eventually saturates to a characteristic signal level σ_{signal} at time $\lesssim T_{90}$, once we begin to run out of correlated variations in the

⁶Recall that the Cauchy-Schwarz inequality states that $|\langle x, y \rangle|^2 \leq \langle x, x \rangle \cdot \langle y, y \rangle$ and that the two sides are equal only if x and y are linearly dependent.

signal.

On intermediate timescales, the slope of $\sigma_{X,\Delta t}$ depends on the shape of the light curve and on the noise spectrum of possible low-level or unresolved flares. If the light curve is correlated on these timescales, which is to say smooth on these timescales, $\sigma_{X,\Delta t}$ will increase as Δt . If, however, the light curve is dominated by the sum of slowly decaying responses to low level flares, a characteristic “flicker noise” spectrum ($PSD(f) \propto 1/f$) may result and $\sigma_{X,\Delta t} \propto \Delta t^0$. Hence, we can test for flaring as a function of timescale by measuring powerlaw $\sigma_{X,\Delta t}$ slopes less than unity.

The fading powerlaw tail of a flare measured with infinite S/N would produce a statistically significant $\sigma_{X,\Delta t}$ for arbitrarily small Δt . These timescales, where $\sigma_{X,\Delta t} \propto \Delta t$, are therefore uninteresting. However, the beginning of a $\sigma_{X,\Delta t} \propto \Delta t^0$ phase yields a physically meaningful timescale for the flaring. The breadth of this phase indicates the range of Δt present in the light curve.

REFERENCES

- Allan, D. W. 1966, Statistics of Atomic Frequency Clocks. Proc. IEEE 31, 221-230
- Band, D., et al. 1993, ApJ, 413, 281
- Barthelmy, S. D., et al. 2005a, 2005, ApJ, 635L, 133
- Barthelmy, S. D., et al. 2005b, Space Sci. Rev., 120, 143-164
- Belli, B. M. 1992, ApJ, 393, 266
- Beloborodov, A. M., Stern, B. E., Svensson, R. 2000, ApJ, 535, 158
- Burrows, D. N., et al. 2005a, Space Sci. Rev., 120, 165-195
- Burrows, D. N., et al. 2005, Science, 309, 1833
- Burrows, D. N., et al. 2007, Submitted to Philosophical Transactions (astro-ph/0701046)
- Unpublished, Presented at the First Glast Symposium, 7 Feb 2007, Palo Alto, CA
- Butler, N. & Kocevski, D. 2007, Submitted to ApJ(astro-ph/0612564)
- Butler, N., Kocevski, D., & Bloom, J. S., in prep.
- Cavallo G, & Rees MJ. 1978, MNRAS, 183, 359

- Chincarini, G., et al. 2007, Submitted to ApJ (astro-ph/0702371)
- Dado, S., Dar, A., & De Rjula, A. 2006, ApJ, 646L, 21 387, 783
- Falcone, A. D., et al. 2006, ApJ, 641, 1010
- Fan, Y. Z. & Wei, D. M., 2005, MNRAS, 364L, 42
- Fenimore et al. 1995, ApJ, 448, L101
- Fenimore, E., Madras, C., Nayakshin, S. 1996, ApJ, 473, 998
- Frontera, F., et al. 2000, ApJSuppl., 127, 59-78
- Gehrels, N., et al. 2004, ApJ, 611, 1005-1020.
- Gendre, B., 2006, A&A 455, 803
- Giblin, T. W., Kouveliotou, C., van Paradijs, J. 1998, AIP conference proceedings, 428, 241G - (4th Huntsville Symposium)
- Granot, J., Knigl, A. & Piran, T. 2006, MNRAS, 370, 1946
- Golensetski, S. V. et al. 1983, Nature, 306, 451
- Hughes, P. A., Aller, H. D., Aller, M. F. 1992, ApJ, 396, 469
- King, A., O'Brien, P. T., Goad, M. R., Osborne, J., Olsson, E., Page, K. 2005, ApJ, 630, 113
- Ioka, K., Kobayashi, S., & Zhang, B. 2005, ApJ, 631, 429
- Kobayashi, S., Piran, T., & Sari, R. 1997, ApJ, 490, 92
- Kocevski, D., Ryde, F., Liang, E. P., 2003, ApJ, 596, 389
- Kocevski, D., Butler, N., & Bloom, J.S. 2006, American Astronomical Society Meeting Abstracts, 209, 22703
- Kolaczyk, E. D., Dixon, D. D. 2000, ApJ, 534, 490
- Krimm, H. A., Granot, J., Marshal, F., Perri, M., Barthelmy, S. D., Burrows, D. N., Gehrels, N., Mszros, P., Morris, D 2007, submitted to ApJ (astro-ph/0702603)
- Kumar, P., & Panaitescu, A., 2000, Ap. J., 541, L51-L54

- Lazzati, D. & Perna, R., 2007, MNRAS, 375L, 46
- Lee, W. & Ramirez-Ruiz, E. 2007, New J.Phys. 9 17 (astro-ph/0701874)
- Liang, E. W., et al. 2006, ApJ, 646, 351
- Lyutikov, M. 2006, MNRAS, 369L, 5
- Mundell, C.G., et al. 2006, Accepted to ApJ (astro-ph/0610660)
- Narayan, R., Paczyński, B., & Piran, T. 1992, ApJ, 395, L83
- Norris, J. P., et. al. 1986, ApJ, 301, 213
- Paczynski B. 1986. Ap. J. Lett. 308:L43
- Panaitescu, A. 2005, MNRAS, 363, 1409
- Perna, R., Armitage, P., Zhang, B., 2006, ApJ, 636, L29
- Piran, T. 1999, PhR, 314, 575
- Press, W. H., et al. 1992, Numerical Recipes in C, (2nd ed.; Cambridge: Cambridge Univ. Press)
- Proga, D. & Zhang, B. 2006 MNRAS, 370, L61
- Ramirez-Ruiz, E., Fenimore, E., 2000, ApJ, 539, 712
- Rees, M. J. & Meszaros, P. 1994, ApJ, 430, L93
- Reichart, D., et al. 2001, ApJ, 552, 57
- Romano, R. 2006, A&A, 456, 917
- Rybicki, G., & Lightman, A. 1979, Radiative Processes in Astrophysics (New York: Wiley)
- Scargle, J. D. 1998, ApJ, 504, 405
- Simonetti, J. H., Cordes, J. M., Heeschen, D. S. 1985, ApJ, 296, 46
- Walker, K. C., Schaefer, B. E., Fenimore, E. E. 2000, ApJ, 537, 264
- Wang, X., & Loeb, A. 2000, ApJ, 535, 788
- Wang, X., Zhuo, L., Mészáros, P. 2006, ApJ, 641, 89

Zhang, B., et al. 2006, ApJ, 642, 354

8. Figure Captions

Fig. 1. - The XRT count rate (cts/s) plotted vs. time since trigger for all 28 flares in 18 separate GRBs. The light curves in this plot are rebinned to $S/N = 10$. A qualitative trend between pulse width and time of peak flux can be seen by inspection.

Fig. 2. - *Top Panel.* A composite BAT and XRT light curve for GRB 060714 showing an increasing pulse duration as a function of time. *Bottom Panel.* The minimum variability timescale in the composite light curve (with power that is at least 3σ above that which is expected from Poissonian fluctuations). The variability of the light curve increases with time, roughly as a powerlaw of $\Delta T_{min} \propto T^{1.9 \pm 0.6}$.

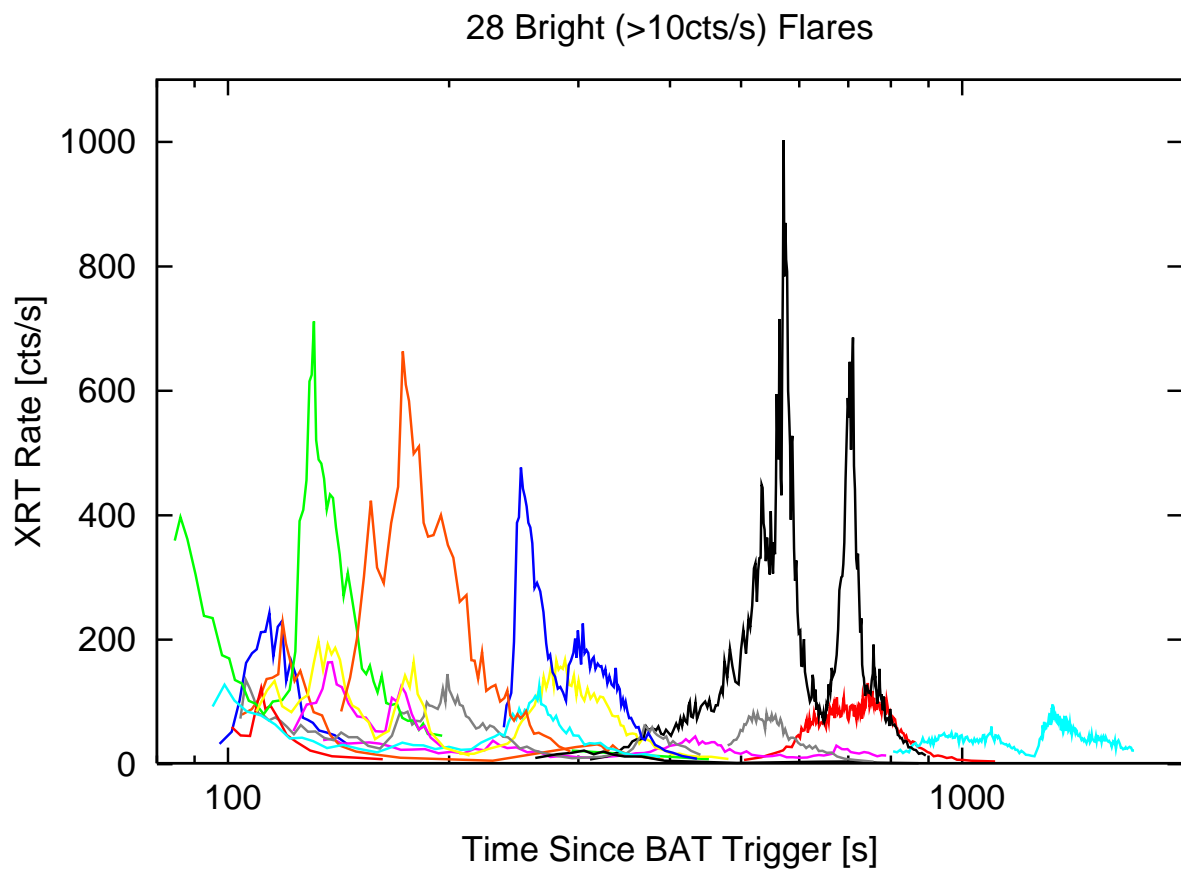
Fig. 3. - The pulse duration T_{90} versus time of peak flux T_p for our entire sample of XRT observed flares. Multiple flares from individual GRBs are displayed with a unique color-symbol combination, whereas GRBs with only one flare are represented by a black diamond. A strong trend ($\tau_K = 0.7$) between pulse width and the time since trigger, as measured in the observer frame, is clear from the data. Only half of the GRBs with multiple flares display a similar increasing pulse duration trend between their associated flares. We conclude that the observed pulse width evolution only becomes apparent when examining durations that cover a broad temporal range.

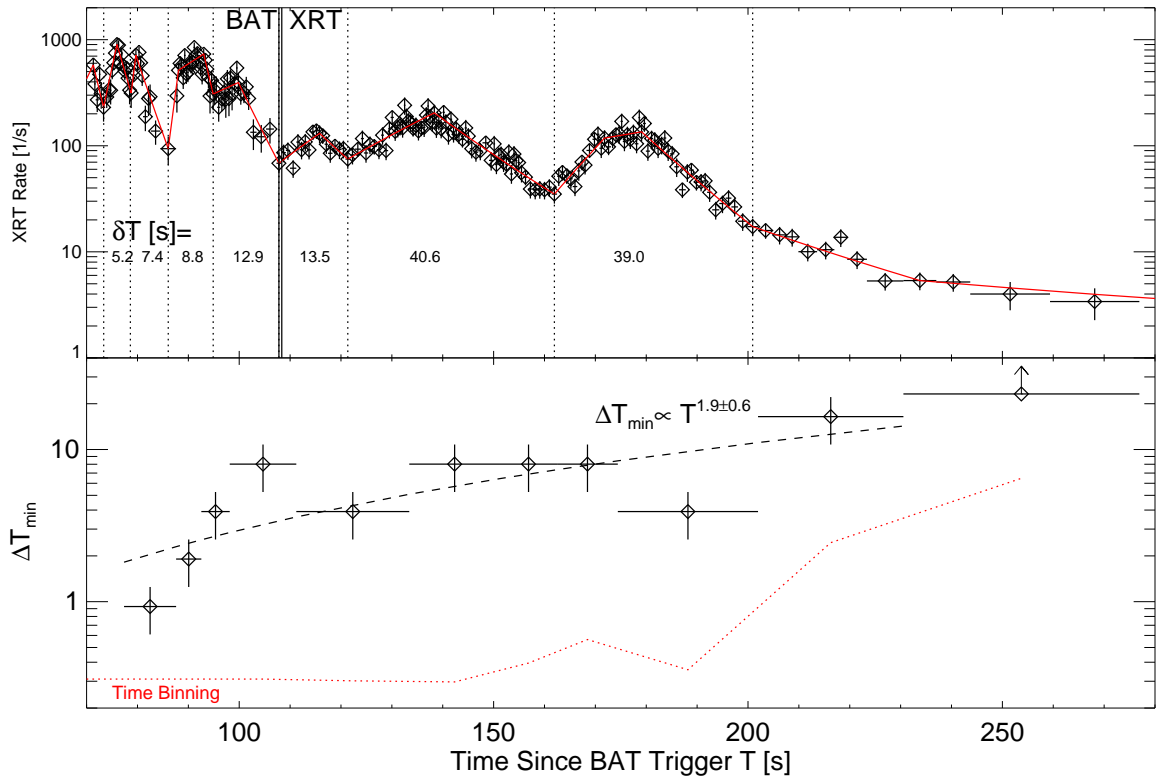
Fig. 4. - Haar wavelet scaleogram $\sigma_{X,\Delta t}$ versus timescale Δt (Panel A) and $\Delta t/t$ (Panel B) for the ensemble of flares under study. The expected level for Poisson noise has been subtracted out. Because $\sigma_{X,\Delta t}$ is calculated from the natural logarithm of the XRT count rate, it can be interpreted as a measure of RMS fractional flux variation versus timescale. The scaleograms reach maximum and turn over on timescales $\Delta t \approx 30 - 300$ s and $\Delta t/t \approx 0.1 - 0.5$, indicating that the flaring occurs on these characteristic timescales. Significant (> 3 -sigma level) variability is observed on timescales $\Delta t \gtrsim 3$ s and $\Delta t/t \gtrsim 0.01$, however, $\sigma_{X,\Delta t} \propto \Delta t$ (dotted red curves) indicates that this variation is due to flaring on intrinsically longer timescales.

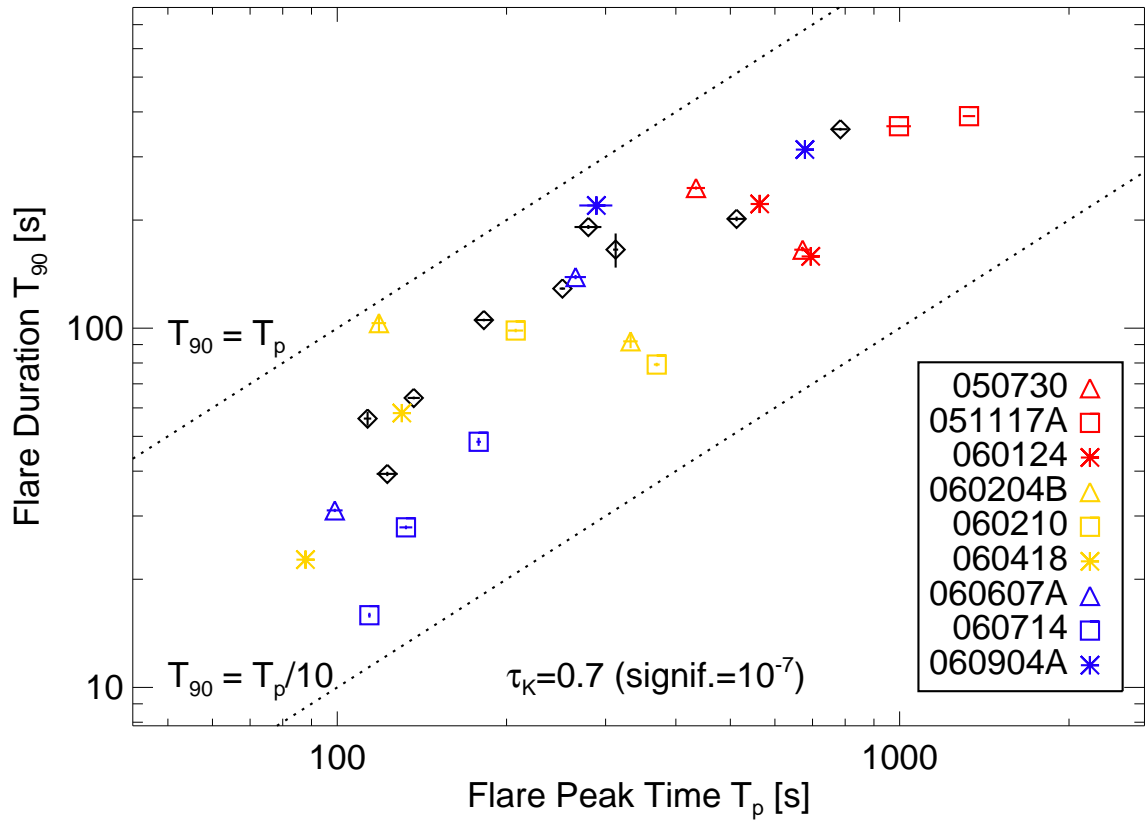
Fig. 5. - The flare rise time T_r plotted vs. the time of peak flux T_p . As in Figure 3, multiple flares from individual GRBs are displayed with a unique color-symbol combination, whereas GRBs with only one flare are represented by a black diamond. An increasing trend

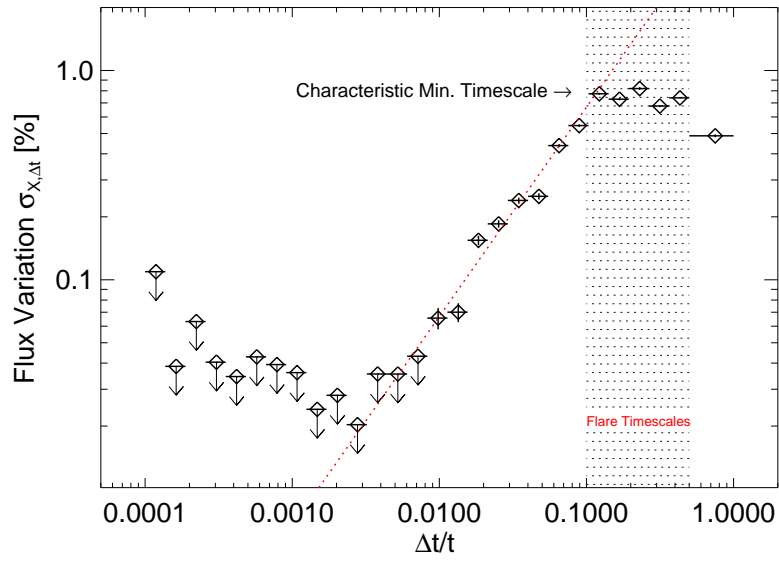
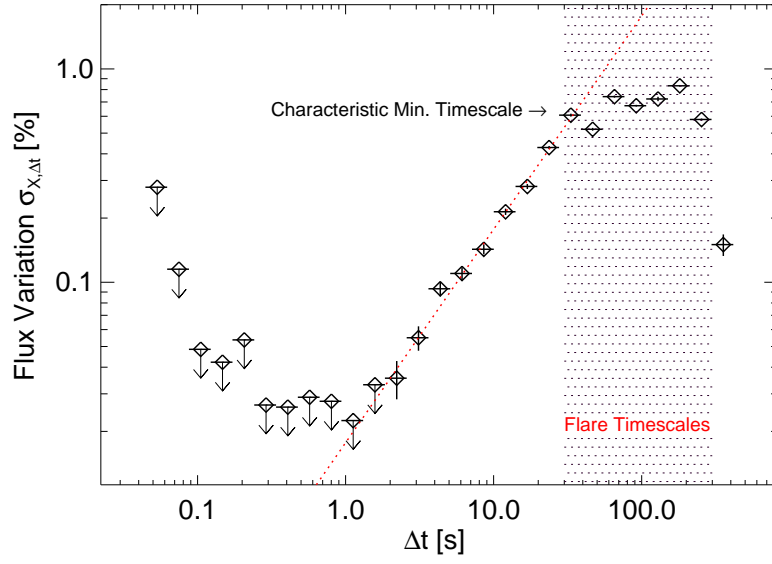
similar to that seen between T_{90} and T_p is evident in the data. The observed rise times are largely insensitive to the effects of background subtraction.

Figures









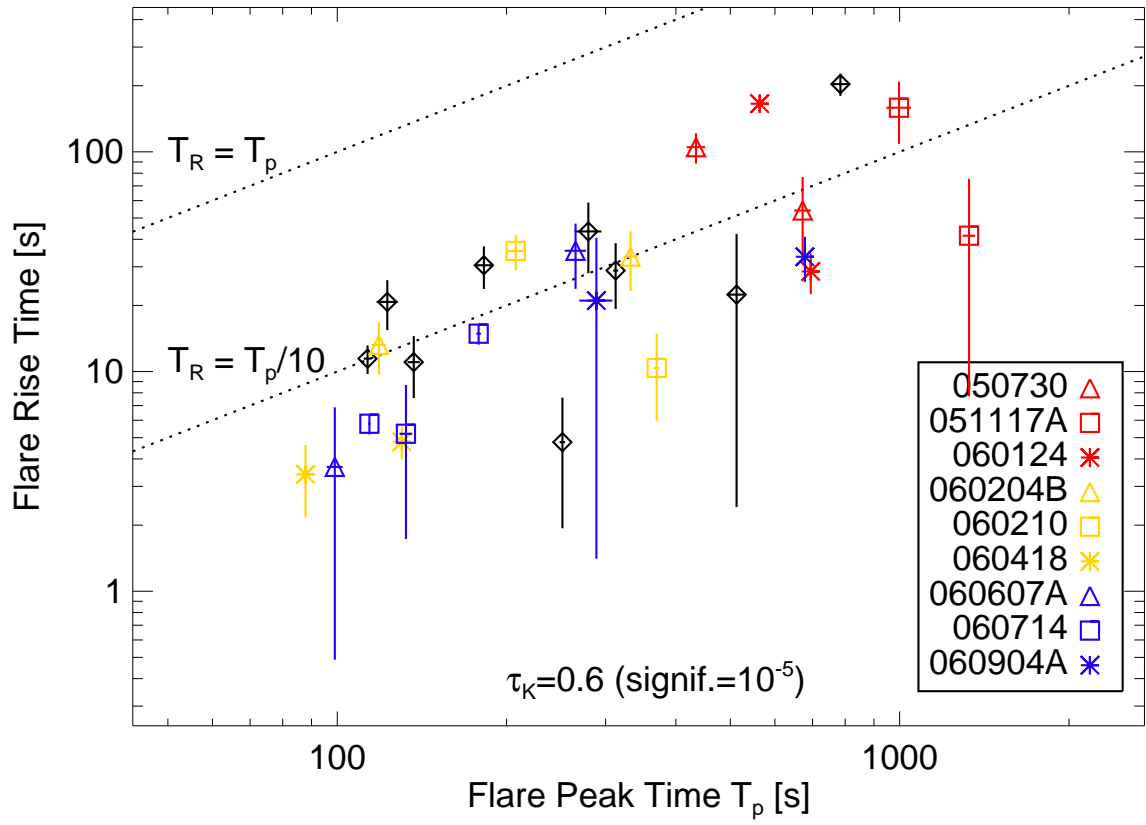


Table 1. Pulse Duration & Time of Peak Flux For Our Entire Sample

| GRB | Time Region (s) | T_{90} (s) | T_{peak} (s) | T_{rise} (s) |
|---------|--------------------|------------------|--------------------------|--------------------------|
| 050502B | 400.0 – 1200.0 | 358.1 ± 3.2 | 784.6 ± 23.7 | 203.5 ± 23.7 |
| 050607 | 250.0 – 600.0 | 165.5 ± 18.0 | 312.6 ± 3.2 | 28.8 ± 9.6 |
| 050713A | 95.0 – 150.0 | 39.3 ± 0.5 | 122.8 ± 5.3 | 20.7 ± 5.3 |
| 060111A | 200.0 – 500.0 | 191.3 ± 2.5 | 279.6 ± 15.4 | 43.4 ± 15.4 |
| 060312 | 100.0 – 200.0 | 56.0 ± 2.5 | 113.2 ± 1.7 | 11.4 ± 1.7 |
| 060526 | 230.0 – 450.0 | 128.9 ± 0.9 | 251.4 ± 2.8 | 4.8 ± 2.8 |
| 060604 | 120.0 – 200.0 | 63.9 ± 0.5 | 136.8 ± 3.4 | 11.0 ± 3.5 |
| 060904B | 140.0 – 300.0 | 105.4 ± 0.8 | 182.3 ± 6.6 | 30.5 ± 6.7 |
| 060929 | 470.0 – 800.0 | 201.5 ± 3.0 | 513.0 ± 19.9 | 22.4 ± 20.0 |
| 050730 | 300.0 – 600.0 | 245.6 ± 2.4 | 434.4 ± 16.3 | 105.1 ± 16.5 |
| 050730 | 600.0 – 800.0 | 165.4 ± 1.7 | 672.2 ± 22.7 | 54.1 ± 22.8 |
| 051117A | 800.0 – 1250.0 | 365.0 ± 1.7 | 997.1 ± 50.0 | 158.9 ± 50.1 |
| 051117A | 1250.0 – 1725.0 | 389.3 ± 1.4 | 1328.3 ± 33.8 | 41.5 ± 33.8 |
| 060124 | 300.0 – 650.0 | 221.7 ± 1.6 | 563.8 ± 7.9 | 165.7 ± 7.7 |
| 060124 | 650.0 – 900.0 | 158.4 ± 1.4 | 694.9 ± 6.0 | 28.5 ± 6.0 |
| 060204B | 100.0 – 270.0 | 103.3 ± 6.4 | 118.6 ± 3.5 | 13.2 ± 3.6 |
| 060204B | 270.0 – 450.0 | 91.9 ± 3.9 | 332.3 ± 9.8 | 33.4 ± 10.1 |
| 060210 | 165.0 – 300.0 | 98.5 ± 1.1 | 207.6 ± 6.5 | 35.4 ± 6.4 |
| 060210 | 350.0 – 450.0 | 79.2 ± 0.9 | 369.9 ± 4.4 | 10.4 ± 4.4 |
| 060418 | 83.0 – 110.0 | 22.7 ± 0.4 | 87.8 ± 1.2 | 3.4 ± 1.2 |
| 060418 | 122.0 – 200.0 | 58.0 ± 0.6 | 130.3 ± 0.8 | 4.8 ± 0.8 |
| 060607A | 93.0 – 130.0 | 31.1 ± 0.3 | 99.0 ± 3.2 | 3.7 ± 3.2 |
| 060607A | 220.0 – 400.0 | 138.8 ± 1.9 | 265.3 ± 11.6 | 35.5 ± 11.7 |
| 060714 | 100.0 – 125.0 | 15.9 ± 0.2 | 114.1 ± 0.6 | 5.8 ± 0.6 |
| 060714 | 125.0 – 160.0 | 27.9 ± 0.3 | 132.5 ± 3.5 | 5.2 ± 3.5 |
| 060714 | 160.0 – 230.0 | 48.3 ± 1.2 | 178.4 ± 1.7 | 14.9 ± 1.6 |
| 060904A | 250.0 – 600.0 | 219.6 ± 12.8 | 288.9 ± 19.5 | 21.0 ± 19.6 |
| 060904A | 600.0 – 1000.0 | 314.2 ± 6.9 | 678.5 ± 7.7 | 33.3 ± 7.7 |

